 CMC, vol.9, no.1, pp.1-24, 2009

A Chain Approach of Boundary Element Row-Subdomains for Simulating the Failure Processes in Heterogeneous Brittle Materials

Zhenhan Yao[1] **and Lingfei Gao**[1]

Abstract: To improve the effectiveness of the lattice model for simulating the failure processes of heterogeneous brittle materials, each lattice element is refined as a subdomain with homogenous material, and is modeled by the boundary element method in this paper. For simplicity, each subdomain is modeled with constant boundary elements. To enhance the efficiency, a row of sub-domains is formed, and then a chain structure of such row-subdomain is constructed. The row-equation systems are solved one by one, and then back substituted, to obtain the final solution. Such a chain subdomain approach of the boundary element method not only reduces the operations, but also the memory requirements. By "failure" of the heterogeneous brittle material is meant to be the debonding of the interface of subdomains, and each homogeneous subdomain remains to be linear elastic. For the simulation of the failure process, a quasi-static approach is adopted. The criterion of interface strength is used to determine the element wherein the interface debonding will occur, and then the interface continuity condition is replaced by the interface debonding condition for the next computation. The simulation of the failure process is controlled by the sequential debonding of the boundary elements. Some results are given to show the applicability of the presented BEM scheme, and the complexity of the failure process of heterogeneous material.

1 Introduction

Based on the advances in computational mechanics, the numerical investigations of heterogeneous materials, including the computation of effective material properties and the simulation of failure process, attracted much attention of researchers and engineers in recent years.

The composite materials, as one type of heterogeneous materials, have been investigated by many researchers in computational mechanics. Most authors adopted the

[1] Department of Engineering Mechanics, Tsinghua University, Beijing, 100084 China

finite element method to simulate the composite materials, for example, Dong and Schmauder (1995), Wulf, Steinkopff and Fischmeister (1996), Ghosh and Moorthy (1998) and Bohm, Han and Eckschlager (2004). Xu, Fan et al (2008) performed FE simulation for bi-continuous heterogeneous solids via a random distribution of materials, to predict the effective elastic properties. In the recent 10 years, some authors adopted the fast multipole boundary element method and have shown some advantageous features in this field, for example, Liu and Nishimura (2005), Wang and Yao (2005) analyzed the 3D fiber- and particle-reinforced composites using FM-BEM, Wang, Yao and Lei analyzed the 2D solids with numerous microcracks using the fast multipole DBEM, and Wang and Yao (2008) simulated the strength of carbon nanotube reinforced composites using rigid-fiber-based BEM.

The rocklike materials and concrete belong to another kind of heterogeneous material. Schlangen and van Mier (1992) presented a simple lattice model for numerically simulating the fracture of concrete materials and structures. Such a simple lattice model is adopted and developed by many authors for simulating the rocklike materials as well. Raghuprasad, Bhat and Bhattacharya (1998) applied the lattice model to simulate the fracture in a quasi-brittle material under direct tension. Tang and Kaiser (1998) presented a numerical approach for the simulation of damage initiation and propagation causing seismic energy release during unstable failure of brittle rock. Chen, Yao and Zheng (2002, 2003) presented 3D numerical simulation of fracture processes in heterogeneous brittle materials using a simple lattice model. Gao, Zheng and Yao (2006) generalized the lattice element to higher order elements considering the influence of stress concentration. Tang, Tham et al (2007) presented some numerical results of the influence of heterogeneity on the strength characterization of rock under uniaxial tension. Liu, Kou, Lindqvist and Tang (2007) presented a series of numerical tests including both rock mechanics, and conducted fracture mechanics tests. Leite, Slowik and Apel (2007) described the computational model of concrete's mesoscopic structure of the simulation of fracture processes.

In simple lattice models, the mechanical property of each lattice is regarded as homogeneous, but the distribution of the properties, including Young's modulus and tensile strength of lattices is random, for example in Weibull or normal distribution. As the deformation of a lattice element reaches the value defined by the failure criterion, as for example that the average principal strain reaches the critical value, the failure of the full lattice is assumed occur and the Young's modulus will be replaced by a small value of 'air modulus'.

On the other hand, the boundary element method has also been developed to deal with the simulation of rocklike heterogeneous materials. Chen, Lin, Yao and Zheng (2003) presented a BEM subdomain approach for the numerical simulation of fail-

ure process in heterogeneous materials. Sfantos and Aliabadi (2007) proposed a multi- scale boundary element modelling for material degradation and fracture of heterogeneous materials, and the microstructural variability of the macro-continuum is considered to investigate the possible applications to heterogeneous materials.

In an earlier investigation of Chen, Lin et al (2003), each lattice element is replaced by a subdomain modeled by the boundary element method, where linear boundary elements are applied, but the failure criterion adopted is still similar to that adopted in a simple lattice model, namely, as the deformation of a BE subdomain reaches the critical value, the whole subdomain is assumed to be damaged, and the Young's modulus is replaced by 'air modulus'.

In this paper, the failure of the heterogeneous brittle material is assumed to be the debonding of the boundary element on the interface of subdomains, and each homogeneous subdomain remains to be linear elastic. The failure criterion is that the interface element will debond, as soon as the average normal traction (or shear stress) on a boundary element reaches the tensile (or shear) strength of the interface or that of the material on the weaker side of the interface. Corresponding to such a failure criterion, the "constant" boundary element is adopted in this paper, rather than linear or higher order elements. In this way, the difficulties caused by the corner conditions of the subdomains can be avoided. To enhance the efficiency, a similar way as presented in Chen, Lin et al (2003) is adopted, a row of subdomains is formed with a row-subdomain at first, and then a chain structure of such row-subdomain is constructed. The row-subdomain equation systems are solved row by row, until the last row, and then back substituted, in order to obtain the final solution. Such a chain approach of row-BE-subdomains not only reduces the operations, but also the memory requirements.

In the next section, the chain approach of BE row-subdomains is formulated, then the algorithm for simulating the failure process of heterogeneous materials is presented, including the failure criterion, modification of the row-BE-subdomain equation systems, and a sequential debonding element controlled simulation of the failure process. After that, some numerical examples are given to show the applicability of the presented approach, and the complexity of the failure process of heterogeneous material.

2 Chain approach of BE row-subdomains

The heterogeneous material is modeled by BE subdomains with n_r rows and n_c columns, each subdomain has the same geometry, same element division and Poisson's ratio, but the Young's modulus could be different, as shown in Fig. 1. Each ingredient of the heterogeneous material could be divided into several subdomains,

or modeled as one subdomain, but one subdomain can not include several ingredients.

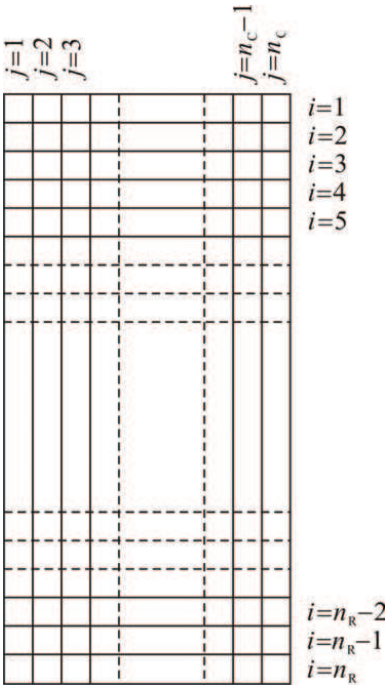

Figure 1: Model of BE sub-domains

The BE equation system of the j-th subdomain in i-th row with Young's modulus $E_{i,j}$ can be formulated as

$$\frac{E_{i,j}}{\bar{E}}\begin{bmatrix}\mathbf{H}_{11} & \mathbf{H}_{12} & \mathbf{H}_{13} & \mathbf{H}_{14}\\ \mathbf{H}_{21} & \mathbf{H}_{22} & \mathbf{H}_{23} & \mathbf{H}_{24}\\ \mathbf{H}_{31} & \mathbf{H}_{32} & \mathbf{H}_{33} & \mathbf{H}_{34}\\ \mathbf{H}_{41} & \mathbf{H}_{42} & \mathbf{H}_{43} & \mathbf{H}_{44}\end{bmatrix}\begin{Bmatrix}\mathbf{u}^{-}_{i,j}\\ \mathbf{u}^{+}_{i,j}\\ \mathbf{u}^{L}_{i,j}\\ \mathbf{u}^{R}_{i,j}\end{Bmatrix}=\begin{bmatrix}\mathbf{G}_{11} & \mathbf{G}_{12} & \mathbf{G}_{13} & \mathbf{G}_{14}\\ \mathbf{G}_{21} & \mathbf{G}_{22} & \mathbf{G}_{23} & \mathbf{G}_{24}\\ \mathbf{G}_{31} & \mathbf{G}_{32} & \mathbf{G}_{33} & \mathbf{G}_{34}\\ \mathbf{G}_{41} & \mathbf{G}_{42} & \mathbf{G}_{43} & \mathbf{G}_{44}\end{bmatrix}\begin{Bmatrix}\mathbf{t}^{-}_{i,j}\\ \mathbf{t}^{+}_{i,j}\\ \mathbf{t}^{L}_{i,j}\\ \mathbf{t}^{R}_{i,j}\end{Bmatrix} \tag{1}$$

where the superscripts $-$, $+$, L and R stand for the upper, lower, left and right side of a row subdomain, the subscript i,j denotes the j-th subdomain in i-th row, all sub-arrays of displacements and tractions consist of the normal components and tangential components of all constant boundary elements. The matrices $\mathbf{H}$ and $\mathbf{G}$ are obtained for the subdomain with certain prescribed Young's modulus $\bar{E}$.

For the first row of BE subdomains, using the continuous condition of the subdo-

mains, the BE equation system can be integrated as

$$\begin{bmatrix} \mathbf{A}_{11}^1 & \mathbf{A}_{12}^1 & \mathbf{A}_{13}^1 & \mathbf{A}_{14}^1 & \mathbf{A}_{15}^1 & \mathbf{A}_{16}^1 \\ \mathbf{A}_{21}^1 & \mathbf{A}_{22}^1 & \mathbf{A}_{23}^1 & \mathbf{A}_{24}^1 & \mathbf{A}_{25}^1 & \mathbf{A}_{26}^1 \\ \mathbf{A}_{31}^1 & \mathbf{A}_{32}^1 & \mathbf{A}_{33}^1 & \mathbf{A}_{34}^1 & \mathbf{A}_{35}^1 & \mathbf{A}_{36}^1 \\ \mathbf{A}_{41}^1 & \mathbf{A}_{42}^1 & \mathbf{A}_{43}^1 & \mathbf{A}_{44}^1 & \mathbf{A}_{45}^1 & \mathbf{A}_{46}^1 \\ \mathbf{A}_{51}^1 & \mathbf{A}_{52}^1 & \mathbf{A}_{53}^1 & \mathbf{A}_{54}^1 & \mathbf{A}_{55}^1 & \mathbf{A}_{56}^1 \\ \mathbf{A}_{61}^1 & \mathbf{A}_{62}^1 & \mathbf{A}_{63}^1 & \mathbf{A}_{64}^1 & \mathbf{A}_{65}^1 & \mathbf{A}_{66}^1 \end{bmatrix} \begin{Bmatrix} \mathbf{u}_1^- \\ \mathbf{u}_{1,1}^L \\ \mathbf{u}_1^I \\ \mathbf{t}_1^I \\ \mathbf{u}_{1,n_C}^R \\ \mathbf{t}_1^+ \end{Bmatrix} = \begin{bmatrix} \mathbf{B}_{11}^1 & \mathbf{B}_{12}^1 & \mathbf{B}_{13}^1 & \mathbf{B}_{14}^1 \\ \mathbf{B}_{21}^1 & \mathbf{B}_{22}^1 & \mathbf{B}_{23}^1 & \mathbf{B}_{24}^1 \\ \mathbf{B}_{31}^1 & \mathbf{B}_{32}^1 & \mathbf{B}_{33}^1 & \mathbf{B}_{34}^1 \\ \mathbf{B}_{41}^1 & \mathbf{B}_{42}^1 & \mathbf{B}_{43}^1 & \mathbf{B}_{44}^1 \\ \mathbf{B}_{51}^1 & \mathbf{B}_{52}^1 & \mathbf{B}_{53}^1 & \mathbf{B}_{54}^1 \\ \mathbf{B}_{61}^1 & \mathbf{B}_{62}^1 & \mathbf{B}_{63}^1 & \mathbf{B}_{64}^1 \end{bmatrix} \begin{Bmatrix} \bar{\mathbf{t}}_1^- \\ \bar{\mathbf{t}}_{1,1}^L \\ \bar{\mathbf{t}}_{1,n_C}^R \\ \mathbf{u}_1^+ \end{Bmatrix} \tag{2}$$

where superscripts $-$, $+$, L and R stand for the upper, lower, left and right side of the row-subdomain, $\mathbf{u}_1^I$, $\mathbf{t}_1^I$ stand for the interface displacements and tractions of the BE subdomains in this row-subdomain, the supper bar of tractions in right side denotes the given value, actually $\bar{\mathbf{t}}_{1,1}^L = \bar{\mathbf{t}}_{1,n_C}^R = \mathbf{0}$. All sub-matrices of $\mathbf{A}$ and $\mathbf{B}$ can be integrated by the sub-matrices of matrices $\mathbf{H}$ and $\mathbf{G}$.

For the next row-subdomains, the BE equation system can be written as

$$\begin{bmatrix} \mathbf{A}_{11}^i & \mathbf{A}_{12}^i & \mathbf{A}_{13}^i & \mathbf{A}_{14}^i & \mathbf{A}_{15}^i & \mathbf{A}_{16}^i \\ \mathbf{A}_{21}^i & \mathbf{A}_{22}^i & \mathbf{A}_{23}^i & \mathbf{A}_{24}^i & \mathbf{A}_{25}^i & \mathbf{A}_{26}^i \\ \mathbf{A}_{31}^i & \mathbf{A}_{32}^i & \mathbf{A}_{33}^i & \mathbf{A}_{34}^i & \mathbf{A}_{35}^i & \mathbf{A}_{36}^i \\ \mathbf{A}_{41}^i & \mathbf{A}_{42}^i & \mathbf{A}_{43}^i & \mathbf{A}_{44}^i & \mathbf{A}_{45}^i & \mathbf{A}_{46}^i \\ \mathbf{A}_{51}^i & \mathbf{A}_{52}^i & \mathbf{A}_{53}^i & \mathbf{A}_{54}^i & \mathbf{A}_{55}^i & \mathbf{A}_{56}^i \\ \mathbf{A}_{61}^i & \mathbf{A}_{62}^i & \mathbf{A}_{63}^i & \mathbf{A}_{64}^i & \mathbf{A}_{65}^i & \mathbf{A}_{66}^i \end{bmatrix} \begin{Bmatrix} \mathbf{u}_i^- \\ \mathbf{u}_{i,1}^L \\ \mathbf{u}_i^I \\ \mathbf{t}_i^I \\ \mathbf{u}_{i,n_C}^R \\ \mathbf{t}_i^+ \end{Bmatrix} = \begin{bmatrix} \mathbf{B}_{11}^i & \mathbf{B}_{12}^i & \mathbf{B}_{13}^i & \mathbf{B}_{14}^i \\ \mathbf{B}_{21}^i & \mathbf{B}_{22}^i & \mathbf{B}_{23}^i & \mathbf{B}_{24}^i \\ \mathbf{B}_{31}^i & \mathbf{B}_{32}^i & \mathbf{B}_{33}^i & \mathbf{B}_{34}^i \\ \mathbf{B}_{41}^i & \mathbf{B}_{42}^i & \mathbf{B}_{43}^i & \mathbf{B}_{44}^i \\ \mathbf{B}_{51}^i & \mathbf{B}_{52}^i & \mathbf{B}_{53}^i & \mathbf{B}_{54}^i \\ \mathbf{B}_{61}^i & \mathbf{B}_{62}^i & \mathbf{B}_{63}^i & \mathbf{B}_{64}^i \end{bmatrix} \begin{Bmatrix} \mathbf{t}_i^- \\ \bar{\mathbf{t}}_{i,1}^L \\ \bar{\mathbf{t}}_{i,n_C}^R \\ \mathbf{u}_i^+ \end{Bmatrix}$$

$$i = 2, 3, ..., n_R \tag{3}$$

However, for the last row-subdomain, the last right-side given variables should be given as: normal displacements of all bottom elements and tangential displacement of the last one element are equal to zero, and tangential tractions of all other elements except the last one are equal to zero.

Solving the equation system (2), the solution can expressed as

$$\begin{Bmatrix} \mathbf{u}_1^- \\ \mathbf{u}_{1,1}^L \\ \mathbf{u}_1^I \\ \mathbf{t}_1^I \\ \mathbf{u}_{1,n_C}^R \\ \mathbf{t}_1^+ \end{Bmatrix} = \begin{Bmatrix} \tilde{\mathbf{u}}_1^- \\ \tilde{\mathbf{u}}_{1,1}^L \\ \tilde{\mathbf{u}}_1^I \\ \tilde{\mathbf{t}}_1^I \\ \tilde{\mathbf{u}}_{1,n_C}^R \\ \tilde{\mathbf{t}}_1^+ \end{Bmatrix} + \begin{bmatrix} \mathbf{D}_1^1 \\ \mathbf{D}_2^1 \\ \mathbf{D}_3^1 \\ \mathbf{D}_4^1 \\ \mathbf{D}_5^1 \\ \mathbf{D}_6^1 \end{bmatrix} \left\{ \mathbf{u}_1^+ \right\} \tag{4}$$

The first array of right side is the part of solution related to the upper side given load, and $\mathbf{u}_1^+$ is the right side unknown, which is dependent on the solution of the subsequent row-subdomains.

Considering the solution of the previous row-subdomains, the equation systems (3) can be rearranged as

$$\begin{bmatrix} \tilde{\mathbf{A}}^i_{11} & \mathbf{A}^i_{12} & \mathbf{A}^i_{13} & \mathbf{A}^i_{14} & \mathbf{A}^i_{15} & \mathbf{A}^i_{16} \\ \tilde{\mathbf{A}}^i_{21} & \mathbf{A}^i_{22} & \mathbf{A}^i_{23} & \mathbf{A}^i_{24} & \mathbf{A}^i_{25} & \mathbf{A}^i_{26} \\ \tilde{\mathbf{A}}^i_{31} & \mathbf{A}^i_{32} & \mathbf{A}^i_{33} & \mathbf{A}^i_{34} & \mathbf{A}^i_{35} & \mathbf{A}^i_{36} \\ \tilde{\mathbf{A}}^i_{41} & \mathbf{A}^i_{42} & \mathbf{A}^i_{43} & \mathbf{A}^i_{44} & \mathbf{A}^i_{45} & \mathbf{A}^i_{46} \\ \tilde{\mathbf{A}}^i_{51} & \mathbf{A}^i_{52} & \mathbf{A}^i_{53} & \mathbf{A}^i_{54} & \mathbf{A}^i_{55} & \mathbf{A}^i_{56} \\ \tilde{\mathbf{A}}^i_{61} & \mathbf{A}^i_{62} & \mathbf{A}^i_{63} & \mathbf{A}^i_{64} & \mathbf{A}^i_{65} & \mathbf{A}^i_{66} \end{bmatrix} \begin{Bmatrix} \mathbf{u}^-_i \\ \mathbf{u}^L_{i,1} \\ \mathbf{u}^I_i \\ \mathbf{t}^I_i \\ \mathbf{u}^R_{i,n_C} \\ \mathbf{t}^+_i \end{Bmatrix} = \begin{bmatrix} \mathbf{B}^i_{11} & \mathbf{B}^i_{12} & \mathbf{B}^i_{13} & \mathbf{B}^i_{14} \\ \mathbf{B}^i_{21} & \mathbf{B}^i_{22} & \mathbf{B}^i_{23} & \mathbf{B}^i_{24} \\ \mathbf{B}^i_{31} & \mathbf{B}^i_{32} & \mathbf{B}^i_{33} & \mathbf{B}^i_{34} \\ \mathbf{B}^i_{41} & \mathbf{B}^i_{42} & \mathbf{B}^i_{43} & \mathbf{B}^i_{44} \\ \mathbf{B}^i_{51} & \mathbf{B}^i_{52} & \mathbf{B}^i_{53} & \mathbf{B}^i_{54} \\ \mathbf{B}^i_{61} & \mathbf{B}^i_{62} & \mathbf{B}^i_{63} & \mathbf{B}^i_{64} \end{bmatrix} \begin{Bmatrix} \tilde{\mathbf{t}}^+_{i-1} \\ \tilde{\mathbf{t}}^L_{i,1} \\ \tilde{\mathbf{t}}^R_{i,n_C} \\ \mathbf{u}^+_i \end{Bmatrix}$$

$$i = 2,3,...,n_R \quad (5)$$

where

$$\left[\tilde{\mathbf{A}}^i_{m1}\right] = \left[\mathbf{A}^i_{m1}\right] + \left[\mathbf{B}^i_{m1}\right]\left[\mathbf{D}^{i-1}_6\right] \quad m = 1,2,...,6 \quad i = 2,3,...,n_R \quad (6)$$

Then the systems can be solved one by one row to get

$$\begin{Bmatrix} \mathbf{u}^-_i \\ \mathbf{u}^L_{i,1} \\ \mathbf{u}^I_i \\ \mathbf{t}^I_i \\ \mathbf{u}^R_{i,n_C} \\ \mathbf{t}^+_i \end{Bmatrix} = \begin{Bmatrix} \tilde{\mathbf{u}}^-_i \\ \tilde{\mathbf{u}}^L_{i,1} \\ \tilde{\mathbf{u}}^I_i \\ \tilde{\mathbf{t}}^I_i \\ \tilde{\mathbf{u}}^R_{i,n_C} \\ \tilde{\mathbf{t}}^+_i \end{Bmatrix} + \begin{bmatrix} \mathbf{D}^i_1 \\ \mathbf{D}^i_2 \\ \mathbf{D}^i_3 \\ \mathbf{D}^i_4 \\ \mathbf{D}^i_5 \\ \mathbf{D}^i_6 \end{bmatrix} \left\{\mathbf{u}^+_i\right\} \quad (7)$$

Until the last row, the give boundary conditions on the lower side of this row should be

$$\begin{Bmatrix} u^+_{\mathrm{n},1} \\ t^+_{\mathrm{t},1} \\ \vdots \\ u^+_{\mathrm{n},k} \\ t^+_{\mathrm{t},k} \\ \vdots \\ u^+_{\mathrm{n},n_c\times n_n-1} \\ t^+_{\mathrm{t},n_c\times n_n-1} \\ t^+_{\mathrm{n},n_c\times n_n} \\ t^+_{\mathrm{t},n_c\times n_n} \end{Bmatrix} = \begin{Bmatrix} 0 \\ 0 \\ \vdots \\ 0 \\ 0 \\ \vdots \\ 0 \\ 0 \\ 0 \\ 0 \end{Bmatrix} \quad (8)$$

Namely, for the numerical experiment of uniaxial tension only the normal displacements are constrained as zero, and the tangential tractions on all other elements

except the last one are given to be zero. The tangential displacement on the last element is set to be zero for the constraint of rigid body displacement. Solving the equation system of the last row-subdomain, the final solution for that row except the tractions on upper side can be obtained. After that, the final solution of each row can be obtained by back substitution. In this way, not only the efficiency of solving the full BE equation systems for heterogeneous material can be enhanced, but also the memory requirement can be reduced.

3 Algorithm for simulating failure process

For simulating the failure process of brittle material, it is assumed that the failure is caused by interface debonding of the subdomains with different or identical material properties. For simplicity, a quasi-static approach is adopted, and the stress singularity at the crack tip is neglected.

As long as the solution of full BE equation systems is obtained, it is not difficult to determine the debonding element according to the criterion

$$k_L \max\left(\frac{t_n^{i,j,k,l}}{\sigma_t^{i,j}},\ \frac{t_t^{i,j,k,l}}{\sigma_s^{i,j}}\right) = 1 \tag{9}$$

where k_L is the load factor to be determined, the superscripts i, j, k, l denote the l-th element on the k-th side of the j-th subdomain in i-th row, $t_n^{i,j,k,l}$, $t_t^{i,j,k,l}$ stand for the normal and tangential traction of each constant boundary element corresponding to unit load applied, $\sigma_t^{i,j}$ and $\sigma_s^{i,j}$ stand for the tensile and shear strength of i-row j-subdomain.

As the debonding at one element occurs, the corresponding interface condition should be changed from continuous to the separated. If the debonding element belongs to the interface of subdomains in the same row, the integrated equation system of this row-subdomain should be modified. If the debonding element belongs to the interface of subdomains in two adjacent rows, then the equation systems of these two row-subdomains should be modified.

For example, if the debonding occurs at the m-th element of upper side of i-th row,

j-th domain, then Eq. (3) should be modified as

$$\begin{bmatrix} \mathbf{A}_{11}^i & \mathbf{A}_{12}^i & \mathbf{A}_{13}^i & \mathbf{A}_{14}^i & \mathbf{A}_{15}^i & \mathbf{A}_{16}^i \\ \mathbf{A}_{21}^i & \mathbf{A}_{22}^i & \mathbf{A}_{23}^i & \mathbf{A}_{24}^i & \mathbf{A}_{25}^i & \mathbf{A}_{26}^i \\ \mathbf{A}_{31}^i & \mathbf{A}_{32}^i & \mathbf{A}_{33}^i & \mathbf{A}_{34}^i & \mathbf{A}_{35}^i & \mathbf{A}_{36}^i \\ \mathbf{A}_{41}^i & \mathbf{A}_{42}^i & \mathbf{A}_{43}^i & \mathbf{A}_{44}^i & \mathbf{A}_{45}^i & \mathbf{A}_{46}^i \\ \mathbf{A}_{51}^i & \mathbf{A}_{52}^i & \mathbf{A}_{53}^i & \mathbf{A}_{54}^i & \mathbf{A}_{55}^i & \mathbf{A}_{56}^i \\ \mathbf{A}_{61}^i & \mathbf{A}_{62}^i & \mathbf{A}_{63}^i & \mathbf{A}_{64}^i & \mathbf{A}_{65}^i & \mathbf{A}_{66}^i \end{bmatrix} \begin{Bmatrix} \mathbf{u}_i^- \\ \mathbf{u}_{i,1}^L \\ \mathbf{u}_i^I \\ \mathbf{t}_i^I \\ \mathbf{u}_{i,n_C}^R \\ \mathbf{t}_i^+ \end{Bmatrix} =$$

$$\begin{bmatrix} \mathbf{B}_{11-}^i & \mathbf{0} & \mathbf{B}_{11+}^i & \mathbf{B}_{12}^i & \mathbf{B}_{13}^i & \mathbf{B}_{14}^i \\ \mathbf{B}_{21-}^i & \mathbf{0} & \mathbf{B}_{21+}^i & \mathbf{B}_{22}^i & \mathbf{B}_{23}^i & \mathbf{B}_{24}^i \\ \mathbf{B}_{31-}^i & \mathbf{0} & \mathbf{B}_{31+}^i & \mathbf{B}_{32}^i & \mathbf{B}_{33}^i & \mathbf{B}_{34}^i \\ \mathbf{B}_{41-}^i & \mathbf{0} & \mathbf{B}_{41+}^i & \mathbf{B}_{42}^i & \mathbf{B}_{43}^i & \mathbf{B}_{44}^i \\ \mathbf{B}_{51-}^i & \mathbf{0} & \mathbf{B}_{51+}^i & \mathbf{B}_{52}^i & \mathbf{B}_{53}^i & \mathbf{B}_{54}^i \\ \mathbf{B}_{61-}^i & \mathbf{0} & \mathbf{B}_{61+}^i & \mathbf{B}_{62}^i & \mathbf{B}_{63}^i & \mathbf{B}_{64}^i \end{bmatrix} \begin{Bmatrix} \mathbf{t}_{i-}^- \\ \mathbf{0} \\ \mathbf{t}_{i+}^- \\ \bar{\mathbf{t}}_{i,1}^L \\ \bar{\mathbf{t}}_{i,n_C}^R \\ \mathbf{u}_i^+ \end{Bmatrix} \quad i = 2,3,...,n_R \tag{10}$$

where the elements in matrix $\mathbf{B}$ corresponding to the debonding element could be replaced by zero, because the debonding element is assumed to be traction free. On the other side of the debonding element, it is at the bottom side of a subregion. The Eq. (3) should be modified as

$$\begin{bmatrix} \mathbf{A}_{11}^i & \mathbf{A}_{12}^i & \mathbf{A}_{13}^i & \mathbf{A}_{14}^i & \mathbf{A}_{15}^i & \mathbf{A}_{16-}^i & -\mathbf{B}_{14*}^i & \mathbf{A}_{16+}^i \\ \mathbf{A}_{21}^i & \mathbf{A}_{22}^i & \mathbf{A}_{23}^i & \mathbf{A}_{24}^i & \mathbf{A}_{25}^i & \mathbf{A}_{26-}^i & -\mathbf{B}_{24*}^i & \mathbf{A}_{26+}^i \\ \mathbf{A}_{31}^i & \mathbf{A}_{32}^i & \mathbf{A}_{33}^i & \mathbf{A}_{34}^i & \mathbf{A}_{35}^i & \mathbf{A}_{36-}^i & -\mathbf{B}_{34*}^i & \mathbf{A}_{36+}^i \\ \mathbf{A}_{41}^i & \mathbf{A}_{42}^i & \mathbf{A}_{43}^i & \mathbf{A}_{44}^i & \mathbf{A}_{45}^i & \mathbf{A}_{46-}^i & -\mathbf{B}_{44*}^i & \mathbf{A}_{46+}^i \\ \mathbf{A}_{51}^i & \mathbf{A}_{52}^i & \mathbf{A}_{53}^i & \mathbf{A}_{54}^i & \mathbf{A}_{55}^i & \mathbf{A}_{56-}^i & -\mathbf{B}_{54*}^i & \mathbf{A}_{56+}^i \\ \mathbf{A}_{61}^i & \mathbf{A}_{62}^i & \mathbf{A}_{63}^i & \mathbf{A}_{64}^i & \mathbf{A}_{65}^i & \mathbf{A}_{66-}^i & -\mathbf{B}_{64*}^i & \mathbf{A}_{66+}^i \end{bmatrix} \begin{Bmatrix} \mathbf{u}_i^- \\ \mathbf{u}_{i,1}^L \\ \mathbf{u}_i^I \\ \mathbf{t}_i^I \\ \mathbf{u}_{i,n_C}^R \\ \mathbf{t}_{i-}^+ \\ \mathbf{u}_{i*}^+ \\ \mathbf{t}_{i+}^+ \end{Bmatrix} =$$

$$\begin{bmatrix} \mathbf{B}_{11}^i & \mathbf{B}_{12}^i & \mathbf{B}_{13}^i & \mathbf{B}_{14-}^i & \mathbf{0} & \mathbf{B}_{14+}^i \\ \mathbf{B}_{21}^i & \mathbf{B}_{22}^i & \mathbf{B}_{23}^i & \mathbf{B}_{24-}^i & \mathbf{0} & \mathbf{B}_{24+}^i \\ \mathbf{B}_{31}^i & \mathbf{B}_{32}^i & \mathbf{B}_{33}^i & \mathbf{B}_{34-}^i & \mathbf{0} & \mathbf{B}_{34+}^i \\ \mathbf{B}_{41}^i & \mathbf{B}_{42}^i & \mathbf{B}_{43}^i & \mathbf{B}_{44-}^i & \mathbf{0} & \mathbf{B}_{44+}^i \\ \mathbf{B}_{51}^i & \mathbf{B}_{52}^i & \mathbf{B}_{53}^i & \mathbf{B}_{54-}^i & \mathbf{0} & \mathbf{B}_{54+}^i \\ \mathbf{B}_{61}^i & \mathbf{B}_{62}^i & \mathbf{B}_{63}^i & \mathbf{B}_{64-}^i & \mathbf{0} & \mathbf{B}_{64+}^i \end{bmatrix} \begin{Bmatrix} \mathbf{t}_i^- \\ \bar{\mathbf{t}}_{i,1}^L \\ \bar{\mathbf{t}}_{i,n_C}^R \\ \mathbf{u}_{i-}^+ \\ \mathbf{0} \\ \mathbf{u}_{i+}^+ \end{Bmatrix} \quad i = 2,3,...,n_R \tag{11}$$

where the unknown in left vector corresponding to the debonding element is changed to the displacements of this side, the corresponding elements in the matrix $\mathbf{A}$ should be replaced by those elements originally in $\mathbf{B}$. And the elements corresponding to the debonding element in matrix $\mathbf{B}$ could be replaced by zero.

Solving the renewed equation systems in above-mentioned way, the next debonding element can be determined.

If the debonding element is located between the neighboring BE subregions in the same row, the original unknown interface variables $\mathbf{u}_i^I$, $\mathbf{t}_i^I$ should be replaced by $\mathbf{u}_i^{\mathrm{I}-}$, $\mathbf{u}_i^{\mathrm{I}+}$, and the corresponding elements in matrix $\mathbf{A}$ should be modified correspondingly.

The failure process is a nonlinear process, but the nonlinearity is caused only by the modification of the configuration corresponding to debonding. For each configuration, either original perfect one or any configuration with debonding, the equation system is still linear. Therefore the numerical simulation of the failure process for such heterogeneous brittle material can be controlled by the sequential debonding elements, rather than applied loading or displacement. For each configuration the computation can be carried out in the same way.

A load-deformation plot obtained by the debonding element controlled failure process is shown in Fig. 2. In the plot each circle point denotes the tensile load applied and the corresponding average normal displacement of the upper loading side for the case of certain element just reached the failure criterion. The line connected these circle point indicates the sequence of the debonding element one by one. The connecting lines in this plot do not have any other essential physical meaning.

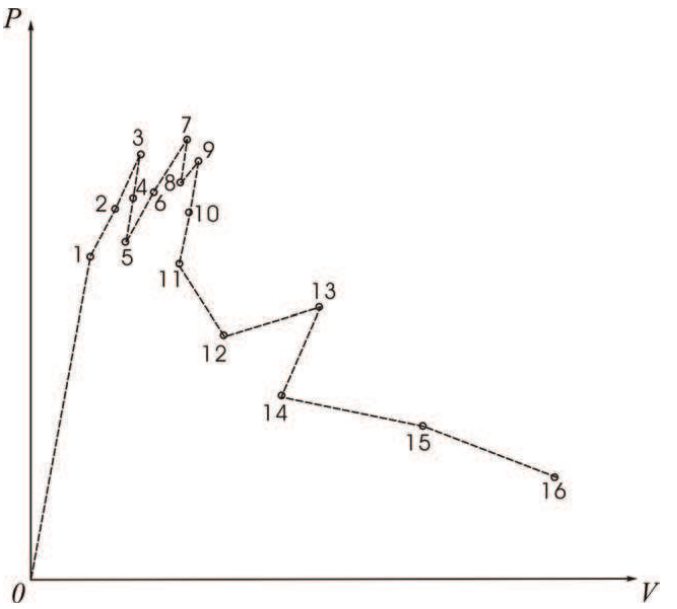

Figure 2: Debonding element controlled load-deformation plot

From this plot, it is not difficult to obtain the corresponding load-deformation curve controlled by applied load or displacement. The applied load controlled load-deformation curve corresponding to Fig. 2 is shown in Fig. 3, and the displacement controlled load-deformation curve is shown in Fig. 4.

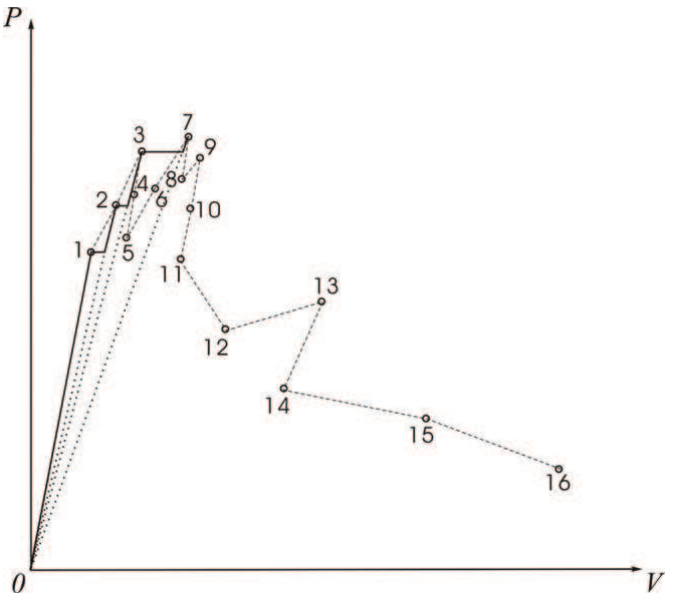

Figure 3: Applied load controlled load-deformation curve

In Fig. 3, it can be observed that only a part of circle points, namely, the points 1, 2, 3, and 7, are related to the load controlled load-deformation curve,. Actually, after the element corresponding to point 3 is debonding, under the corresponding load level, the next elements corresponding to the points 4, 5, 6 will be debonded immediately, because the debonding load is lower than the current load. As the applied load controlled load-deformation curve reaches the point 7, the plate will fully lost the load-carrying ability, and the curve is stop there.

In Fig. 4, similar feature can be observed. The points 4, 5, 8, 10, 11 and 14 are not related to the displacement controlled load-deformation curve. Actually, after the element corresponding to the point 3 is debonding, the elements corresponding to the points 4 and 5 will be debonded immediately.

Certainly, it should be pointed out here, these curves are come from the numerical simulation, rather than physical experiments. The numerical simulation is based on the above mentioned basic assumptions, all dynamic factors are neglected.

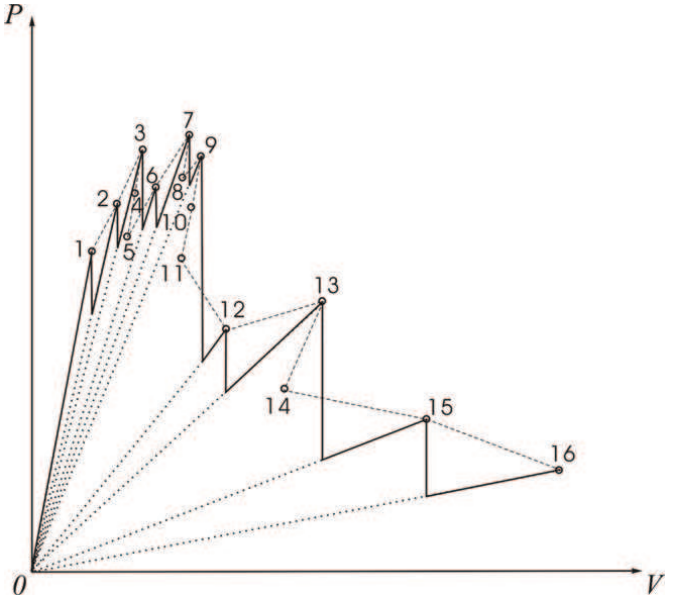

Figure 4: Displacement controlled load-deformation curve

4 Numerical examples

4.1 Effective Young's modulus for test samples of heterogeneous square sheet

Five test sample groups of heterogeneous brittle square sheet with 20×20 ingredients are computed using the above mentioned BE subdomain approach. The shape parameterγ of the Weibull distribution of Young's modulus for each groups are taken as 2.0, 3.0, 4.0, 5.0 and 10.0 respectively, and the scale parameter α is always taken as 1.0. The Young's moduli of the ingredients are created by Matlab with function weibrnd (1.0, γ, 20, 20). Each group has 10 samples. The random distribution of the Young's modulus for some samples is illustrated in Fig. 5. Some numerical results are listed in Table 1, and the relationship of the average value of effective Young's moduli versus the shape parameterγ of the Weibull distribution is shown in Fig. 6.

From the results listed in Table 1, it can be concluded that for the computation of the effective Young's modulus of such heterogeneous materials, each ingredient modeled as one BE subdomain with one constant element on each side is good enough, and each ingredient divided into one subdomain with 4 constant element on each side is more accurate. The variance for larger sample with 40×40 ingredients is less than smaller one, and the average value of 10 sample with 20×20 ingredients

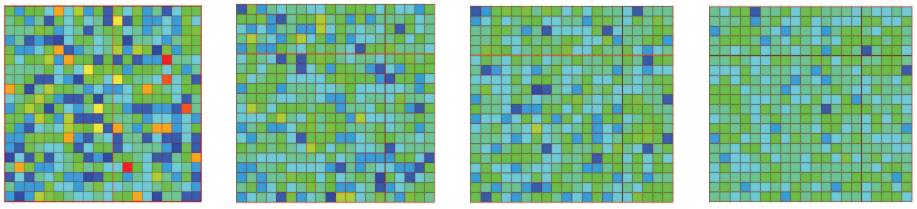

(a) γ= 2.0 (b) γ= 3.0 (b) γ= 4.0 (b) γ= 5.0

Figure 5: Random distribution of Young's modulus for samples with different shape parameter

is accurate enough.

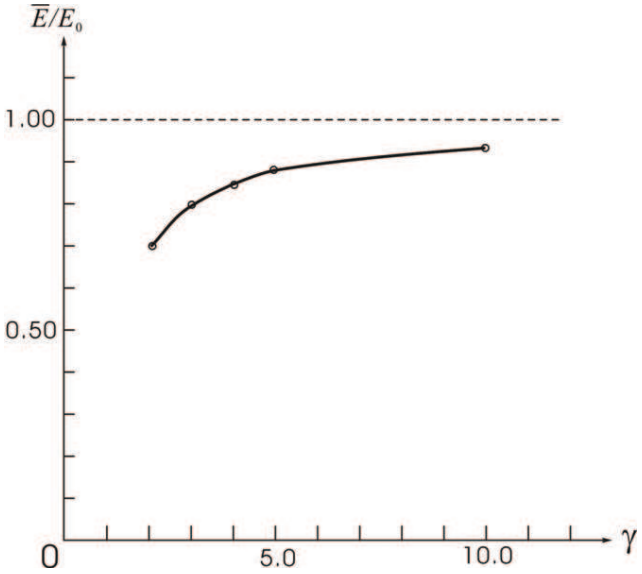

Figure 6: The relationship of effective Young's moduli versus the shape parameter γ

The relationship of effective Young's moduli versus the shape parameter of Weibull distribution shows that the heterogeneity of the material reduces the Young's modulus, and the effective Young's modulus will approach that of the corresponding homogeneous material, as the shape parameter of the Weibull distribution increases.

Table 1: Numerical results of nondimensional effective Young's moduli

γ	Ingredients	Mesh of an ingredient		Sample										$\bar{E}/E_0$
		Subdomain	Element per side	1	2	3	4	5	6	7	8	9	10	
2.0	20×20	1	1	0.713	0.679	0.718	0.676	0.722	0.710	0.674	0.727	0.717	0.702	0.704
		2×2	1	0.728	0.696	0.734	0.694	0.740	0.728	0.693	0.744	0.734	0.720	0.721
		4×4	1	—	—	—	—	—	—	—	—	—	0.719	—
		1	2	0.708	0.669	0.710	0.668	0.704	0.709	0.660	0.720	0.712	0.695	0.696
		2×2	2	0.710	0.672	0.712	0.671	0.709	0.711	0.665	0.721	0.714	0.698	0.698
		1	4	0.707	0.673	0.715	0.672	0.717	0.709	0.675	0.725	0.717	0.704	0.701
	40×40	1	1	0.710	0.692	0.706	0.702	0.696	0.702	0.715	0.691	0.702	0.711	0.703
3.0	20×20	1	1	0.806	0.805	0.813	0.808	0.791	0.813	0.787	0.777	0.768	0.808	0.798
4.0	20×20	1	1	0.844	0.833	0.856	0.832	0.850	0.851	0.858	0.862	0.852	0.848	0.852
5.0	20×20	1	1	0.909	0.870	0.895	0.876	0.870	0.877	0.873	0.894	0.891	0.879	0.883
10.0	20×20	1	1	0.943	0.935	0.940	0.927	0.939	0.939	0.944	0.945	0.929	0.944	0.939

4.2 Simulation of the failure process for a test sample of square sheet with 10×10 ingredients using different discretization schemes

A small test sample is used to simulate the failure process of heterogeneous brittle material, which is consisted of 10×10 ingredients with a Weibull distribution of shape parameter $\gamma = 2.0$, created by Matlab with the function of weibrnd (1.0, 2.0, 10, 10). Each ingredient is modeled as single BE subdomain, 2×2 and 4×4 subdomains with one constant element on each side respectively, or as single BE subdomain with 4 constant elements on each side.

For the simulation, the distribution of tensile strength is assumed to be related with the distribution of Young's moduli, namely in the computation the tensile strength is assumed to be 0.1% of Young's modulus, and the shear strength is assumed to be 70% of tensile strength. For reference, the distribution of the Young's modulus is shown in Fig. 7

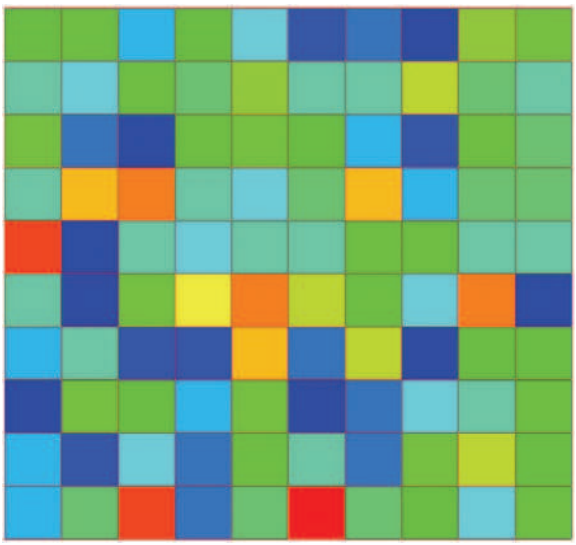

Figure 7: Distribution of Young's modulus

The comparison of the failure process simulated using different discretization schemes, by the plot of debonding interface elements, is shown in Fig. 8. Because the numerical error of the computation could influence the sequentially cracked interface, the plots of debonding interface elements obtained for different discretization schemes are not identical. But the failure is initiated and propagated mostly in the same weaker ingredients.

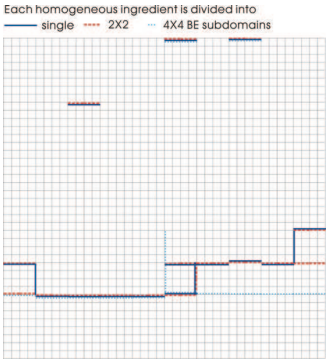

(a) different subdomain division

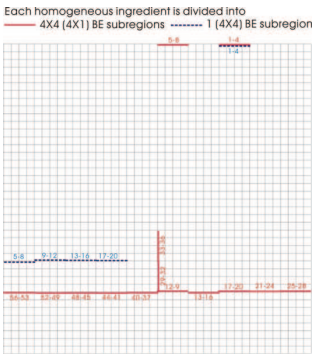

(b) different discretization with same element length

Figure 8: Comparison of the failure process simulated using different discretization schemes

Fig. 8(b) shows the comparison of the failure process for different discretization with identical element length, namely, each ingredient divided into 4×4 subdomains with one constant element on each side, and modeled as single subdomain with 4 constant elements on each side. The stress distribution obtained by the latter scheme should be more accurate. Considered the higher stress near the crack tip, the failure of this sample is approximately the initiation and propagation of single crack. But after debonding of 20 elements some numerical instability happened for the latter scheme. This problem should be further investigated in future, and in the following numerical examples the subdomains with one element on each side will be adopted for simulating the failure process of heterogeneous brittle materials, and it is numerically stable in the computation of all numerical examples.

The debonding element controlled load-deformation plot for different discretization schemes are shown in Fig. 9(a). The corresponding tensile load controlled load-deformation curves are shown in Fig. 9(b). It can be observed that the tensile strengths obtained by different discretization schemes are different. The highest is obtained by the scheme of single subdomain with one element per side for each ingredient, then 2×2, 4×4 subdomain schemes, the lowest value is obtained by the scheme of single subdomain with 4 element per side. The values of the tensile strength of this test sample obtained by the above mentioned schemes are 3254, 3165, 2986 and 2413 respectively.

Because finer mesh for BE subdomains can obtain more accurate results for the stress analysis, therefore the lowest value should be a better approximation of the tensile strength. The real fracture analysis with boundary element method can ob-

tain further improved results, but the cost would be too high. The presented scheme with single subdomain per ingredient with one element per side is already better than simple lattice model for such kind of brittle failure.

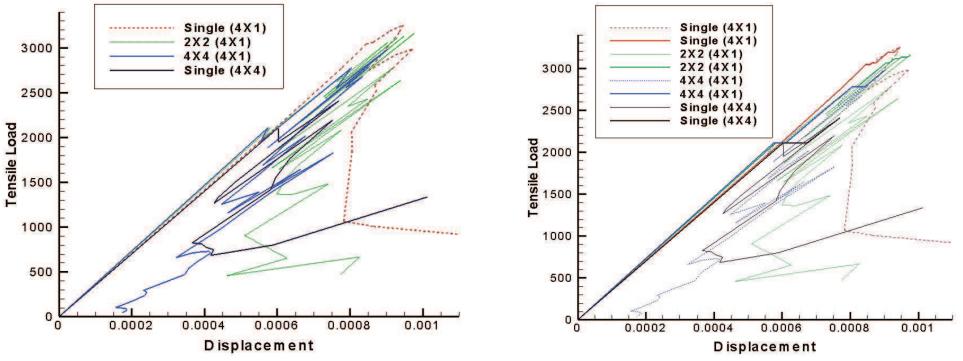

(a) debonding element controlled plot (b) tensile load controlled plot

Figure 9: Load-deformation plot of the test sample

4.3 Failure process of a rectangular sheet with 15×125 ingredients

The test sample in the last numerical example consists of only 10×10 ingredients. Therefore the characteristics of the brittle failure is quite similar with the homogeneous material, it is approximately the initiation and propagation of single crack. To simulate the characteristics of the brittle failure of heterogeneous material, larger test sample is required.

As a test sample, a rectangular sheet with 15×125 ingredients is adopted, the Weibull distribution of the material properties, namely, Young's modulus, and the related tensile strength and shear strength, is created by Matlab with the function weibrnd (1.0, 1.5, 15, 125). To avoid the debonding on traction loaded side, an additional row of subregions with homogeneous higher Young's modulus is added there.

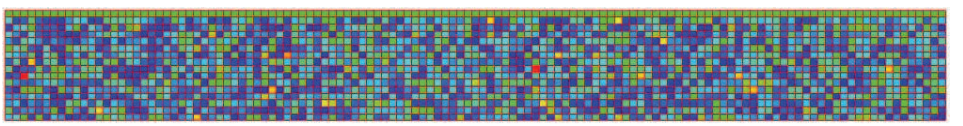

Figure 10: Weibull distribution of Young's modulus

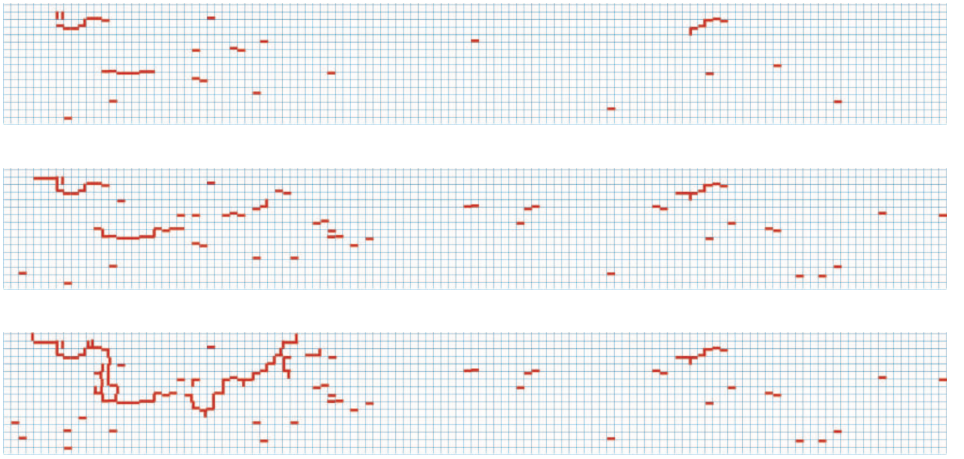

Figure 11: Three stages of the failure process: 40, 80 and 130 elements debonding

The distribution of Young's modulus is shown in Fig. 10, and the failure process simulated is shown in Fig. 11 with the plot of debonding elements in three stages: 40 elements debonding, 80 elements debonding and 130 elements debonding.

These plots have shown the characteristics of the failure of heterogeneous material. The debonding occurs at dispersive location and unlike the initiation and propagation of single crack for homogeneous material under simple tensile loading. The computation is stable until 130 elements debonding and a part of test sample loses the necessary geometrical constraint.

The debonding element controlled load-deformation plot is shown in Fig. 12(a), where the multi-peaks corresponding to the dispersive interface cracks in heterogeneous material can be observed. It is quite different from the plot for homogeneous sheet with 20×20 subregions under simple tension shown in Fig. 12(b). However, other characteristics of the failure of heterogeneous materials observed in displacement controlled experiment, such as the softening stage of the load-deformation curve or residual strength, still can not be found here.

4.4 Tensile strength for test samples of heterogeneous square sheet

To investigate the effect of heterogeneity on the tensile strength, one more test sample groups of heterogeneous brittle square sheet with 20×20 ingredients than that presented in example 1 for the computation of effective Young's modulus, are simulated using the presented approach. Each ingredient is modeled as single subdomain with one constant boundary element per edge. The upper side of the

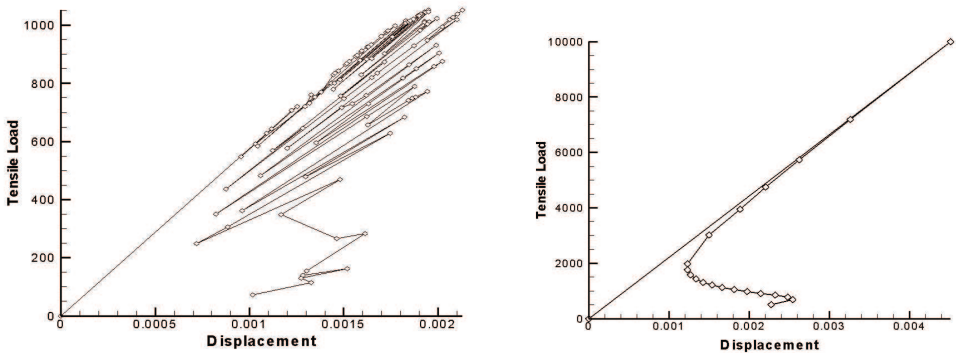

Figure 12: Debonding element controlled load-deformation plot for test sample and 20×20 homogeneous one

sample is uniformly normal traction loaded.

For the simulation, the same assumption as above mentioned has been adopted. The distribution of tensile strength is assumed to be related with the distribution of Young's modulus, namely in the computation the tensile strength is assumed to be 0.1% of Young's modulus, and the shear strength is assumed to be 70% of tensile strength.

The nondimensional tensile strength obtained is listed in Table 2. It can be observed that the tensile strength decreases as the heterogeneity increases, namely the shape parameter γ of Weibull distribution decreases. Furthermore, in comparison with Table 1, it can be observed that the decrease of tensile strength is much more remarkable than the decrease of effective Young's modulus. For example, in the case of $\gamma = 10.0$, the tensile strength is reduced 36.3% in comparison with corresponding homogeneous material, while the effective Young's modulus only reduced 6.1%; for the case of $\gamma = 2.0$, the tensile modulus reduced 75.6%, effective Young's modulus reduced only 29.6%.

For different samples with identical shape parameter γ of Weibull distribution the variances of the nondimensional tensile strength is also listed in Table 2. The variances listed are not too big for the samples with 20×20 ingredients. However the difference of the corresponding debonding element controlled load-deformation plot and the plot of debonding interface element are remarkable.

The debonding element controlled load-deformation plots for 10 samples of $\gamma = 1.5$ are shown in Fig. 13, and the corresponding plots of debonding interface element are shown in Fig. 14.

In Fig. 13(e) the remarkable softening stage and residual strength can be observed,

Table 2: Numerical results of nondimensional tensile strength

γ	Ingredients	Sample										$\bar{\sigma}_b^e/\sigma_b^0$	Variance
		1	2	3	4	5	6	7	8	9	10		
1.5	20×20	0.233	0.188	0.183	0.181	0.160	0.207	0.193	0.170	0.179	0.166	0.186	0.020
2.0	20×20	0.281	0.264	0.244	0.236	0.196	0.281	0.270	0.250	0.229	0.240	0.244	0.023
3.0	20×20	0.349	0.379	0.328	0.319	0.322	0.342	0.357	0.307	0.327	0.353	0.338	0.020
4.0	20×20	0.404	0.447	0.381	0.387	0.367	0.381	0.415	0.362	0.387	0.443	0.397	0.028
5.0	20×20	0.468	0.434	0.460	0.408	0.500	0.466	0.461	0.452	0.530	0.513	0.469	0.035
10.0	20×20	0.602	0.605	0.676	0.612	0.647	0.671	0.586	0.669	0.681	0.619	0.637	0.034

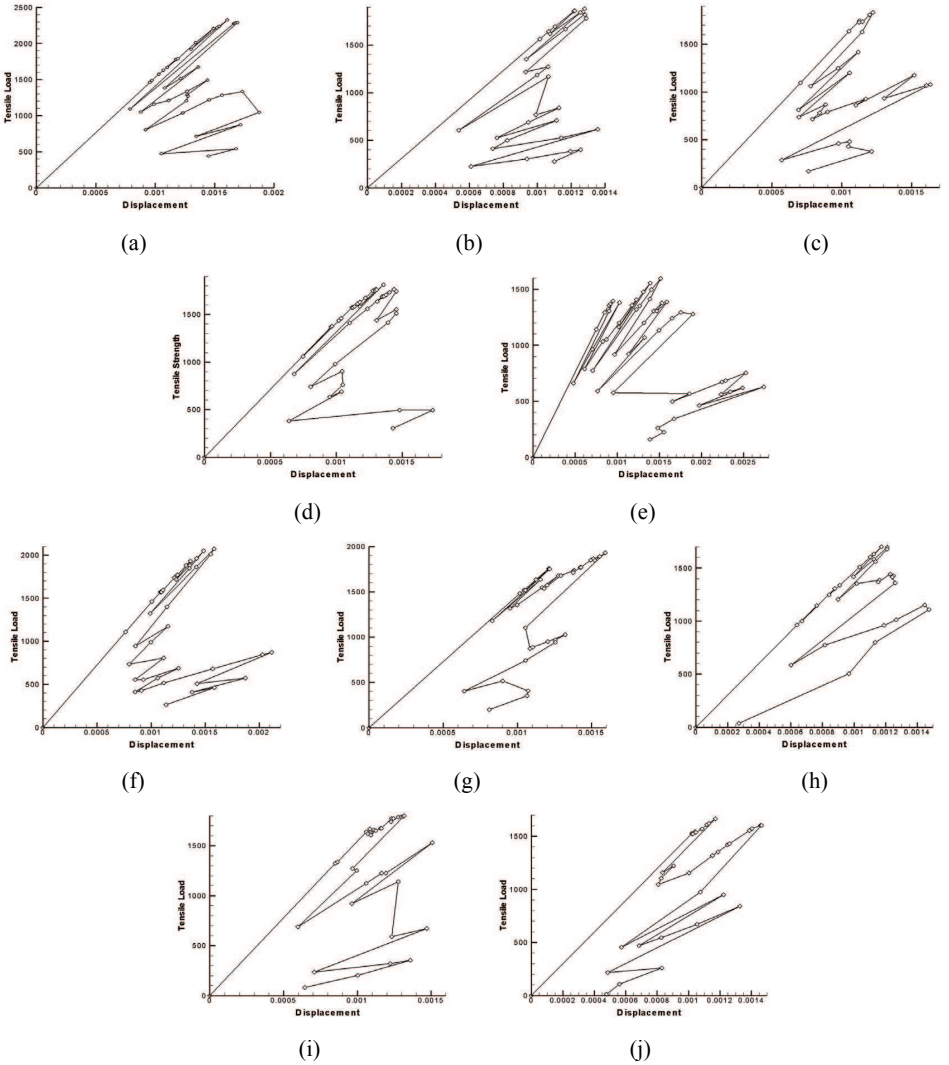

Figure 13: Debonding element controlled load-deformation plots for different samples of $\gamma = 1.5$

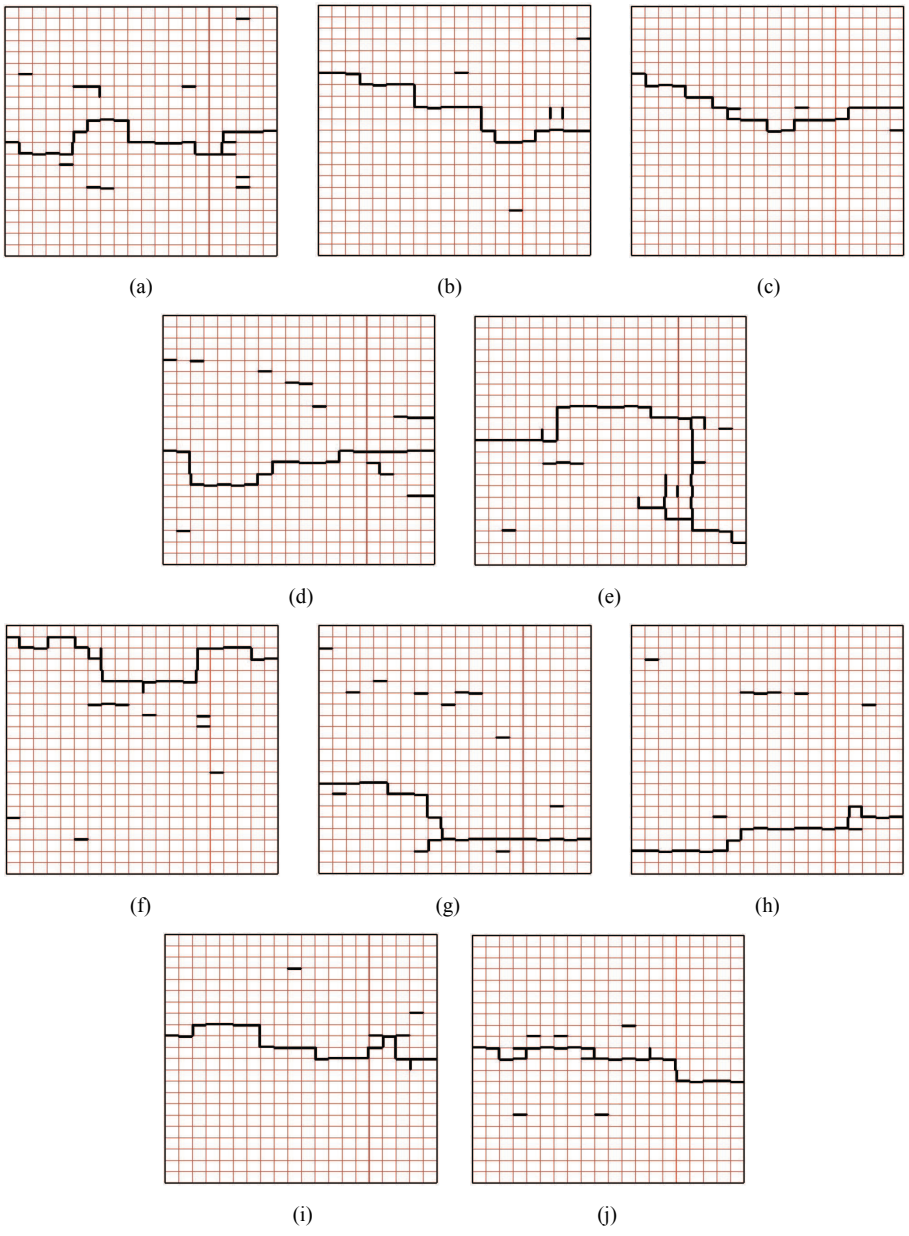

Figure 14: Plots of debonding interface element for different samples of $\gamma = 1.5$

and the corresponding plot of debonding interface elements has shown dispersive characteristics. However, the plots of other samples, such as Fig. 13(a, b, g), have not shown any softening characteristics, and some plots of debonding interface elements have shown that the failure process is similar to the initiation and propagation of single crack. These results have shown the complexity of the failure process of heterogeneous brittle material.

5 Concluding Remarks

A chain approach of BE row-subdomains, for simulating the failure process of heterogeneous brittle materials, is presented in this paper, wherein each ingredient is modeled with BE subregion or subregions, and the boundary of each subregion is divided into constant boundary elements. The constant boundary element adopted in this approach not only avoids the difficulties caused by the corner conditions in subdomain approach, but also matches to the failure criterion adopted in this paper.

The failure of the heterogeneous brittle material is modeled with sequential debonding of the interfacial boundary elements, as the boundary traction reaches the failure criterion. This model is more reasonable than the sequential failure of the whole BE subregions or of the whole simple lattice element as presented in most prior literature.

Considering that the nonlinearity of the failure process of heterogeneous brittle material is caused by the element-debonding-based configuration changes, after the last element cracks and before the debonding of the next element, the equation system for a fixed configuration is still linear, a sequential debonding element controlled algorithm for the simulation of failure process is suggested in this paper. From the debonding element controlled load-deformation plot, it is not difficult to transform it into a traction controlled load-deformation curve or displacement controlled load-deformation curve.

Some numerical examples for the computation of effective elastic properties and the simulation of the failure process of the heterogeneous materials are given to show the effectiveness and applicability of the presented numerical approach, and the complexity of the failure process of heterogeneous brittle material.

Further investigations should be focused on the validation of the presented approach with the experimental results of real heterogeneous materials.

References

Bohm, H. J., Han, W., Eckschlager, A. (2004): Multi-inclusion unit cell studies of reinforcement stresses and particle failure in discontinuously reinforced ductile

matrix composites, *CMES: Computer Modeling in Engineering & Science*, Vol. 5, pp. 5-20.

Chen, Y. Q., Yao, Z. H., Zheng, X. P. (2002): 3-D numerical simulation of fracture processes in heterogeneous brittle materials, *Acta Mechanica Solida Sinica*, Vol. 15, pp. 332-341.

Chen, Y. Q., Yao, Z. H., Zheng, X. P. (2003): Theoretical statistical solution and numerical simulation of heterogeneous brittle materials, *Acta Mechanica Sinica*, Vol. 19, pp. 276-284.

Chen, Y. Q., Lin, C. Y., Yao, Z. H., Zheng, X. P. (2003): BEM for numerical simulation of failure process in heterogeneous materials, *Engineering Mechanics*, Vol. 20, pp. 19-25 (in Chinese).

Dong, M., Schmauder S. (1996): Transverse mechanical behaviour of fiber reinforced composites – FE modelling with embedded cell models, *Computational Materials Science*, Vol. 5, pp. 53-66.

Gao, L. F., Zheng, X. P., Yao, Z. H. (2006): Numerical simulation of elastic behaviour and failure processes in heterogeneous material, *CMC: Computers Materials & Continua*, Vol. 3, pp. 25-36.

Ghosh, S., Moorthy, S. (1998): Particle fracture simulation in non-uniform microstructures of metal-matrix composites, Acta Materialia, Vol. 46, pp.965-982.

Leite, J. P. B., Slowik, V., Apel, J. (2007): Computational model of mesoscopic structure of concrete for simulation of fracture processes, *Computers & Structures*, Vol. 85, pp. 1293-1303.

Liu, H. Y., Kou, S. Q., Lindqvist, P. A., Tang, C. A. (2007): Numerical modelling of the heterogeneous rock fracture process using various test techniques, *Rock Mechanics and Rock Engineering*, Vol. 40, pp. 107-144.

Liu, Y. J., Nishimura, N., Otani, Y. et al. (2005): A fast boundary element method for the analysis of fiber-reinforced composites based on a rigid-inclusion model, *Journal of Applied Mechanics – Transactions of the ASME*, Vol. 72, pp. 115-128.

Raghuprasad, B. K., Bhat, D. N., Bhattacharya, G. S. (1998): Simulation of fracture in a quasi-brittle material in direct tension – a lattice model, *Engineering Fracture Mechanics*, Vol. 61, pp. 445-460.

Schlangen E., van Mier J. G. M. (1992): Simple lattice model for numerical simulation of fracture of concrete materials and structures, *Materials and Structures*, Vol. 25, pp. 534-542.

Sfantos, G. K., Aliabadi, M. H. (2007): Multi-scale boundary element modelling of material degradation and fracture, *Computer Methods in Applied Mechanics and*

Engineering, Vol. 196, pp. 1310-1329.

Tang, C. A. (1998): Numerical simulation of cumulative damage and seismic energy release during brittle rock failure, *International Journal of Rock Mechanics and Mining Sciences*, Vol. 35, pp. 113-121.

Tang, C. A., Tham, L. G., Wang S. H., Liu, H., Li, W. H. (2007): A numerical study of the influence of heterogeneity on the strength characterization of rock under uniaxial tension, Mechanics of Materials, Vol. 39, pp. 326-339.

Wang, H. T., Yao, Z. H. (2005): A new fast multipole boundary element method for large scale analysis of mechanical properties in 3D particle-reinforced composites, *CMES: Computer Modeling in Engineering & Science*, Vol. 7, pp. 85-95.

Wang, H. T., Yao, Z. H. (2008): A rigid-fiber-based boundary element model for strength simulation of carbon nanotube reinforced composites, *CMES: Computer Modeling in Engineering & Science*, Vol. 29, pp. 1-14.

Wang, P. B. Yao, Z. H., Lei, T. (2006): Analysis of solids with numerous microcracks using the fast multipole DBEM, *CMC: Computers Materials & Continua*, Vol. 3, pp. 65-75.

Wulf, J., Steinkopff, Th., Fischmeister, H. F. (1996): FE-simulation of crack paths in the real microstructure of an Al(6061)/SiC composite, *Acta Materialia*, Vol. 44, pp. 1775-1779.

Xu, L. M., Fan, H., Xie, X. M., Li, C. (2008): Effective elastic property estimation for bi-continuous heterogeneous solids, *CMC: Computers Materials & Continua*, Vol. 7, pp. 119-127.